Available online at www.sciencedirect.com
SCIENCE DIRECT®
Applied Surface Science xxx (2006) xxx–xxx
applied surface science
www.elsevier.com/locate/apsusc

Analysis of codeposited Gd_2O_3/SiO_2 composite thin films by phase modulated spectroscopic ellipsometric technique

N.K. Sahoo *, R.B. Tokas [1], S. Thakur [1]

Spectroscopy Division, Bhabha Atomic Research Centre, Trombay, Mumbai 400 085, India

Received 8 June 2005; received in revised form 23 January 2006; accepted 7 March 2006

Abstract

Tailoring of the refractive index of optical thin films has been a very fascinating as well as challenging topic for developing new generation optical coatings. In the present work a novel Gd_2O_3/SiO_2 composite system has been experimented and probed for its superior optical properties through phase modulated spectroscopic ellipsometry, spectrophotometry and atomic force microscopy. The optical parameters of the composite films have been evaluated using Tauc–Lorentz (TL) formulations. In order to derive the growth dependent refractive index profiles, each sample film has been modeled as an appropriate multilayer structure where each sub-layer was treated with the above TL parameterizations. All codeposited films demonstrated superiority with respect to the band gap and morphological measurements. At lower silica mixing compositions such as in 10–20% level, the composite films depicted superior spectral refractive index profile, band gap as well as the morphology. This aspect highlighted the fact that microstructural densifications in composite films can override the chemical compositions while deciding the refractive index and optical properties in such thin films.

PACS: 42.79.Wc; 78.66.−w; 78.20.Ci; 61.16.Ch; 51.70.+f; 52.70.Kz

Keywords: Optical coatings; Codeposition; Electron beam evaporation; Thin film multilayers; Ellipsometry; Spectrophotometry; Atomic force microscopy; Composite films

1. Introduction

Tailoring of the refractive index of optical thin films has been the subject of research for various optical thin film applications such as integrated optical waveguides, rugate filters, antireflection, wavelength multiplexers and Raman notch filters [1,2]. The recent emergence of novel optical design concepts using gradient and inhomogeneous index profiles emphasizes the importance of studying mixed composition optical thin films [3–6]. The coevaporation technique utilizing high and low index materials to form microscopically continuous, graded-index thin film structures has become a most popular approach to such research problems. The proper composition, and thus refractive index, is achieved by appropriately controlling the relative deposition rates of the constituent materials. This alloying or mixing of materials increases the range of properties that is unavailable from a finite number of discrete thin film materials [7]. These properties are not only intermediate to those of the constituents of the alloy but often are also unique and unobtainable by any single material. For example various high temperature phases with superior film qualities can be attainable in ZrO_2 at relatively lower substrate temperatures with appropriate admixture of Y_2O_3, Sc_2O_3, CaO, etc. [8,9].

Mixed composition systems derived through codeposition processes behave in unique ways and each system must be studied independently to determine the overall film properties. A typical representation of the electron beam reactive codeposition process is depicted in Fig. 1. It can be seen in

* Corresponding author. Tel.: +91 22 25593871; fax: +91 22 25505151.
E-mail address: nksahoo@apsara.barc.ernet.in (N.K. Sahoo).
[1] Fax: +91 22 25505151.

0169-4332/$ – see front matter © 2006 Elsevier B.V. All rights reserved.
doi:10.1016/j.apsusc.2006.03.013

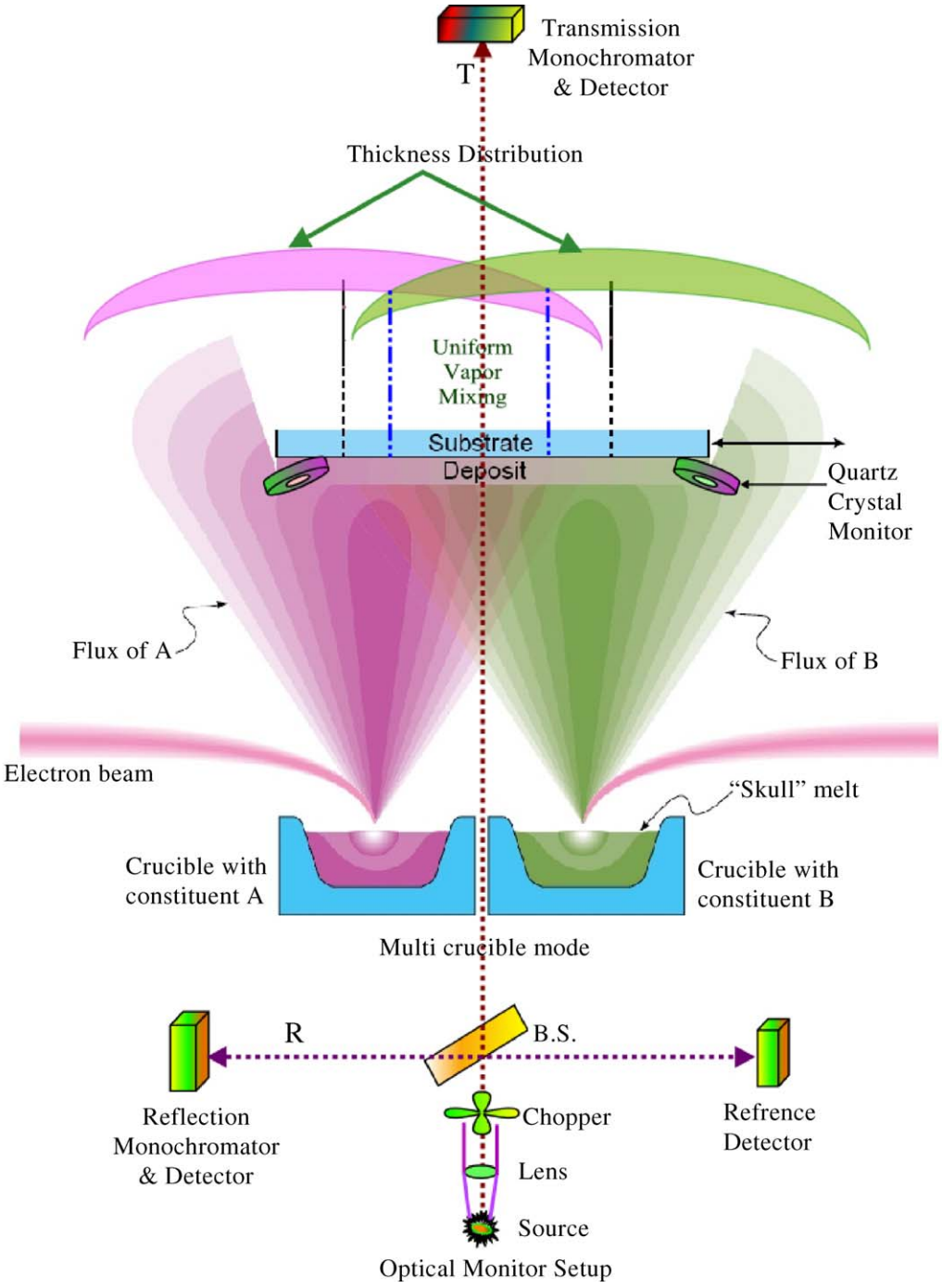

Fig. 1. A typical pictorial representation of a reactive electron beam codeposition process depicting the different zones of the vapour mixing and monitoring.

this figure that there are several zones in the vapour mixings and one can select an appropriate region as per the need of the application. Although refractive indices of mixed composition films often vary somewhat linearly with atomic composition, the mechanical and structural properties generally do not and therefore cannot be predicted based on those of the pure constituents. This behavior is due to the fact that the microstructure, which strongly affects mechanical properties, does not vary linearly with the composition. Factors such as bond strengths, chemical environment of the atoms and grains, surface mobility of the species during deposition and both short- and long-range order can induce a microstructure that is unique to the mixed composition film [5,10]. For example, the composition dependence of intrinsic stress shows linear behavior in layered films but non-linear in codeposited films in mixtures of Ge with ZnS, CdTe, MgF_2 and CeF_3 [11]. In the present work also it has been noticed that the presence of certain volume mixture of

SiO_2 in Gd_2O_3 has improved the refractive index, which is representative of the density as well as polycrystalline phase of the material.

With respect to optical coating applications, only a handful of thin film materials have been experimented in order to achieve the refractive index tunability. There have been several research experiments concerning the most popular TiO_2–SiO_2 system [5,12,13]. This system has an advantage of giving wide range of index tunability. However, the applicability of this composite system is limited to visible and near infrared wavelength region only, due to their band gap constraints. Crystallization and phase segregation in codeposited and alternating layered TiO_2–SiO_2 films were studied by X-ray diffraction and TEM analysis [14]. The addition of small amounts of a glass forming solute (e.g., SiO_2) into some oxides has reported to prevent crystallization of the host material. Admixture of SiO_2 into sputter deposited TiO_2 films was also observed to retard crystallization [15–17]. Below certain critical thickness (~500 Å) crystallization in pure TiO_2 films is reported to be inhibited [18]. This has been attributed to the increasing role of surface energy as the area-to-volume ratio increases with decreasing film thickness. This implies that different ratios in mixing of the component materials can lead to different type of outcome in the evolution in microstructural as well as optical properties.

In this work on a novel Gd_2O_3/SiO_2 composite thin film system similar effects are noticed in various films codeposited with different component ratios. It is worth mentioning that the gadolinia–silica (Gd_2O_3/SiO_2) combinations have recently drawn attention to develop deep ultraviolet optical coatings especially for excimer laser applications [19–21]. In the present study it is observed that it is possible to achieve a superior band gap in codeposited films so that its application can be extended well below the ArF laser (193 nm) wavelength. Presently only fluorides with poor index contrasts are being used to develop optical filters and coatings in this deep or extreme ultraviolet (DUV/EUV) spectral region [22–26]. The present codeposited system can be conveniently used to meet such challenging task through its superior properties related to refractive index as well as band gap tunability. Besides the index tunability, like most codeposited films, the present composite films have also demonstrated superior microstructural and morphological properties [27].

The most interesting result in the microstructural properties of the present gadolinia–silica system is noticed at mixing ratios of 90:10 and 80:20 for Gd_2O_3:SiO_2 composition. Not only the refractive index increased to a better value than the pure Gd_2O_3 but also a superior topography with more dense and fine morphological features was distinctly noticed. Although the mean index for each composite film follows a systematic somewhat linear trend with respect to the mixing ratios, a more detailed probe in to the microstructure revealed interesting growth dependent non-linear behaviours in the spectral refractive index profiles. The appearance of such non-linear behaviour may be attributed to either due to the growth dependent microstructural changes or process-instability or combinations of both. Such changes have been very conveniently modeled through the phase modulated spectroscopic ellipsometric technique using Tauc–Lorentz (TL) parameterization.

2. Tauc–Lorentz formulations for Gd_2O_3/SiO_2 codeposited system

Recent progress in ellipsometry instrumentation permits precise measurement and characterization of optical coating materials in the deep-UV wavelength range. Dielectric coating materials exhibit their first electronic interband transition in this spectral range. The Tauc–Lorentz model is a powerful tool with which it has now become extremely convenient to parameterize interband absorption above the band edge [28]. Although this model was derived for amorphous semiconductor, it can be conveniently applied to polycrystalline and nanocrystalline thin films as well [29]. For example to model the dielectric functions in HfO_2 films, the Tauc–Lorentz dispersion was successfully adopted for the amorphous and polycrystalline films by Cho et al. [30]. The application of this model for the parameterization of the optical absorption of TiO_2, Ta_2O_5, HfO_2, Al_2O_3 and LaF_3 polycrystalline thin-film materials has been described by von Blanckenhagen et al. [31].

In Tauc–Lorentz (TL) formulation, for semiconductors and insulators, the imaginary part of the dielectric constant is determined by multiplying the Tauc joint density of states by ε_2 obtained from the Lorentz oscillator model. The imaginary part of the dielectric constant is given as following [32]:

$$\varepsilon_{2\mathrm{TL}}(E) = \left[\frac{AE_0C(E-E_g)^2}{(E^2-E_0^2)+C^2E^2}\frac{1}{E}\right], \quad E > E_g, \tag{1}$$

$$\varepsilon_{2\mathrm{TL}}(E) = 0, \quad E \le E_g \tag{2}$$

The subscript TL indicates that the model is based on the Tauc joint density of state and Lorentz oscillator; the four fitting parameters are E_g, A, E_0 and C, and all are in units of energy [33]. All these parameters have very special significances and contribute immensely to the dielectric function. For instance, E_0 is the peak transition energy, E_g the band gap energy and C is a broadening parameter, which can be related to the degree of disorder in the material. A is another parameter which is proportional to the height of ε_2, related to the film density. The real part of the dielectric function ε_1 is obtained by Kramers–Kroning integration, given by [34]:

$$\varepsilon_1 = \xi(\infty) + \frac{2}{\pi}P\int_{E_2}^{\infty}\frac{\xi\varepsilon_2(\xi)}{\xi^2-E^2}\,\mathrm{d}\xi, \tag{3}$$

where the P stands for Cauchy principal part of the integral and an additional fitting parameter $\varepsilon_{1\mathrm{TL}}(\infty)$ has been included. The integral is taken over the positive energies. The

integral can be solved in closed form and can be given by [35]:

$$\varepsilon_{1TL}(E) = \varepsilon_{1TL}(\infty) + \frac{1}{2}\frac{A}{\pi}\frac{C}{\varsigma^4}\frac{a_{ln}}{\alpha E_0}\ln\left[\frac{E_0^2+E_g^2+\alpha E_g}{E_0^2+E_g^2-\alpha E_g}\right] - \frac{A}{\pi.\varsigma^4}\frac{a_{tan}}{E_0}\left[\pi - a\tan\left(\frac{2E_g+\alpha}{C}\right) + a\tan\left(\frac{-2E_g+\alpha}{C}\right)\right] + 2\frac{AE_0}{\pi\varsigma^4\alpha} - \left\{E_g(E^2-\gamma^2)\left[\pi + 2a\tan\left(2\frac{\gamma^2-E_g^2}{\alpha C}\right)\right]\right\} - \frac{AE_0C}{\pi\varsigma^4}\frac{E^2+E_g^2}{E}\ln\left(\frac{|E-E_g|}{E+E_g}\right) + 2\frac{AE_0C}{\pi\varsigma^4}E_g\ln\left[\frac{|E-E_g|(E+E_g)}{\sqrt{(E_0^2-E_g^2)^2+E_g^2C^2}}\right] + 2\frac{AE_0C}{\pi\varsigma^4}E_g\ln\left[\frac{|E-E_g|(E+E_g)}{\sqrt{(E_0^2-E_g^2)^2+E_g^2C^2}}\right] \quad (4)$$

where

$$a_{ln} = (E_g^2-E_0^2)E^2 + E_g^2C^2 - E_0^2(E_0^2+3E_g^2), \quad (5a)$$

$$a_{tan} = (E-E_0^2)(E_0^2+E_g^2) + E_g^2C^2, \quad (5b)$$

$$\varsigma^4 = (E^2-\gamma^2)^2 + \frac{\beta^2C^2}{4}, \quad (5c)$$

$$\beta = \sqrt{4E_0^2-C^2}, \qquad \gamma = \sqrt{\frac{E_0^2-C^2}{2}} \quad (5d)$$

Although the TL expression (Eqs. (1)–(3)) is empirical, it does satisfy the major criteria for models of most thin film dielectric functions. The TL expression is consistent with known physical phenomena, within the limitations of the model. Also, it should be mentioned that the TL model does not account for any absorption below the band gap, nor does it possess the correct high frequency limit. But in case of our present composite thin film system, the model has provided several useful information and parameters consistent with the results of the complementary characterization techniques.

For the present codeposited composite Gd_2O_3/SiO_2 system one has to consider an effective dielectric function ε if the individual dielectric strengths are ε_g and ε_s for Gd_2O_3 and SiO_2, respectively. The effective dielectric strength ε is then given by [36]:

$$\varepsilon = \frac{1}{2}\left\{\varepsilon_g + \frac{c_s}{1-L}(\varepsilon_s-\varepsilon_g) - \varepsilon_s\frac{L}{1-L} + \left[\left(\varepsilon_s\frac{L}{1-L} - \varepsilon_g\frac{c_s}{1-L}(\varepsilon_s-\varepsilon_g)\right)^2 + 4\varepsilon_g\varepsilon_s\frac{L}{1-L}\right]^{1/2}\right\} \quad (6)$$

This expression gives the dielectric constant of the composite thin film medium consisting of spheroidal particles of dielectric constant ε_s embedded in a dielectric constant of ε_g or vice versa. The shape of the spheroidal particles is described in terms of a form factor L, which assumes values 0 and 1.

With these parameterizations, the refractive index n_f and extinction coefficient k_f of the codeposited Gd_2O_3/SiO_2 films obey the following equation:

$$\hat{n}_f = n_f + ik_f = \sqrt{\hat{\varepsilon}(E)} \quad (7)$$

where

$$\hat{\varepsilon} = \varepsilon_1 + i\varepsilon_2 \quad (8)$$

With this substitution, the film refractive index $n_f(E)$, absorption coefficient $k_f(E)$ and absorption constant $\alpha(E)$ can be established from,

$$n_f(E) = \left\{\frac{[(\varepsilon_1^2+\varepsilon_2^2)^{1/2}+\varepsilon_1]}{2}\right\}^{1/2} \quad (9)$$

$$k_f(E) = \left\{\frac{[(\varepsilon_1^2+\varepsilon_2^2)^{1/2}-\varepsilon_1]}{2}\right\}^{1/2} \quad (10)$$

$$\alpha(E) = \frac{4\pi k_f(E)}{\lambda} = \left(\frac{2E}{\hbar c}\right)\left\{\frac{[(\varepsilon_1^2+\varepsilon_2^2)^{1/2}-\varepsilon_1]}{2}\right\}^{1/2} \quad (11)$$

The inhomogeneities of the codeposited films are given by a profile of the complex refractive index $\hat{n}_f$ across these films. Such inhomogeneities have been probed using appropriate multilayer models.

For our present Gd_2O_3/SiO_2 system, most of the composite films under TL formulations have demonstrated very small numerical values for the parameter "*C*", which implied a highly ordered structure in all these films with respect to their pure counterparts. The parameter "*A*" which is the representation of film density has shown substantial higher values for the codeposited films especially with a Gd_2O_3:SiO_2 compositions as 60:40. The pure gadolinia films demonstrated higher disorder parameter as well as lower film density and lower band gap values. By codeposition, all these microstructural parameters have been substantially improved depicting better film properties [37]. Some of the earlier research publications have very emphatically stated the microstructural densifications and void fraction reductions of composite films leading to superior refractive index and microstructural properties [38–40]. So it can be easily inferred that by addition of SiO_2 in Gd_2O_3 matrix, not only it lead to refractive index tunability but also superior stabilized composite phases are resulted. The mean refractive index profiles of pure Gd_2O_3 film and composite films of compositions 90:10 and 80:20 of Gd_2O_3:SiO_2 have been depicted in Fig. 2. It can be distinctly noticed that the addition of 10–20% SiO_2 in to the Gd_2O_3 system has enhanced the packing density and there by the spectral refractive index. Subsequent sections highlight more details on the experimental aspects of this codeposition process.

3. Experimental

Under the present investigation, we have carried out some systematic experiments and analysis of co-deposited thin films

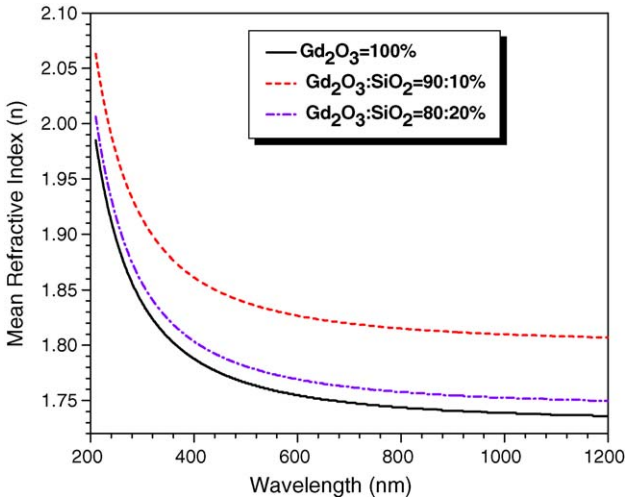

Fig. 2. Spectral mean refractive index profiles of the pure Gd_2O_3 and the composite Gd_2O_3/SiO_2 thin films with the composition ratios of 90:10 and 80:20. Composite film with 10% and 20% silica components have depicted a superior refractive index values supporting the morphological measurements presented in subsequent figures.

of Gd_2O_3/SiO_2 system using phase modulated ellipsometry, spectrophotometry and multimode scanning probe microscope techniques. However, as mentioned above this research paper predominantly presents the results of ellipsometric measurements and analyses. The samples were deposited in a fully automatic thin film vacuum system ''VERA-902'' by adopting the reactive electron beam deposition technique. The depositions of the films were carried out using two 8KW VTD electron beam guns with sweep and automatic emission controls. The film materials for SiO_2 and Gd_2O_3 were chosen from Cerac's batch number ''S-1060'' (purity 99.99%) and ''G-1076'' (purity 99.9%), respectively. The substrate temperature was maintained at 70 °C for the deposited films. The total pressure inside the chamber during the deposition process was maintained at 1×10^{-4} mbar through MKS mass flow controllers. The constituents of the gases present during the deposition were analyzed by a residual gas analyzer (RGA) model; Pffeier's Prisma-200. The film thicknesses were monitored both using the Leybold's OMS-2000 optical thickness monitor (OTM) as well as Inficon's XTC/2 quartz crystal monitors (QCM). The individual rates of depositions were very accurately monitored as well as controlled in automatic mode as per the requirements of the co-deposition process. The proportional, integration and differential (PID) parameters of the thickness as process control system were judiciously optimized in order to avoid unwanted rate fluctuations during codeposition processes. By such appropriate and accurate rate controls, it was possible to obtain Gd_2O_3/SiO_2 codeposited composite films with the desired compositions in the ranges of 10–90%. The entire deposition process parameters such as substrate temperature, optical thicknesses, rates of deposition, total reacting gas pressure were monitored and controlled by a Siemen's industrial programmable logic controller (PLC) with appropriate front-end software. The co-deposited film optical thicknesses were decided to remain 6–8 quarter wave in order to obtain appropriate numbers of interference fringes for spectrophotometric as well as ellipsometric analysis techniques.

For ellipsometric studies, Jobin Yvon's phase modulated spectroscopic ellipsometer model UVISEL has been employed to analyze the growth dependent spectral optical properties. As described above Tauc–Lorentz (TL) formulation has been adopted to probe the co-deposited films for their refractive index profile using a discrete multilayer approach. For AFM characterization, NT-MDT's solver P-47H multimode ambient-based scanning probe system has been utilized. The cantilever used was a Si_3N_4 with typical spring constant of 0.6 N/m and resonant frequency of 75 KHz. We have adopted the contact mode operation without any image filtering technique for the topographic measurements. For Fourier analysis, the built-in FFT module of the control software ''NOVA-SPM'' was employed to generate the mappings. In order to have the consistency in the experimental results, the same cantilever was used for all the topographic measurements. All the co-deposited films were spectrally measured for their reflectance as well as transmittance characteristics using Shimadzu UV3101PC spectrophotometer system equipped with an integrating sphere accessory. The results of various characterization techniques have been presented in the subsequent section.

4. Results and discussions

In the present experiment, several codeposited films with the Gd_2O_3/SiO_2 compositions (Fig. 1) in the mixing range of 10:90–90:10 have been prepared under certain predefined substrate temperature and oxygen partial pressure conditions decided through previous experiments. As mentioned above, in Fig. 2 the spectral refractive index profiles of pure Gd_2O_3 and codeposited Gd_2O_3/SiO_2 with the compositions of 90:10 and 80:20 have been depicted. In this figure it can be noticed the

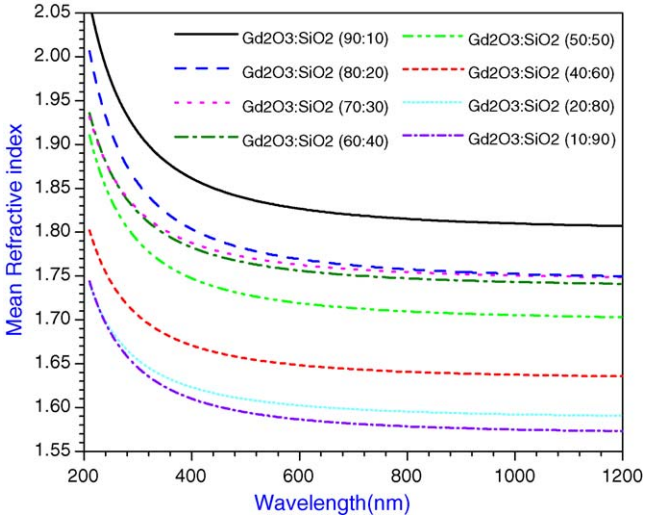

Fig. 3. Spectral mean refractive index profiles of the codeposited composite Gd_2O_3/SiO_2 thin films with various composition ratios in the mixing ratio ranges of 90:10–10:90. The computed mean refractive indices follow a systematic trend as per their mixing compositions.

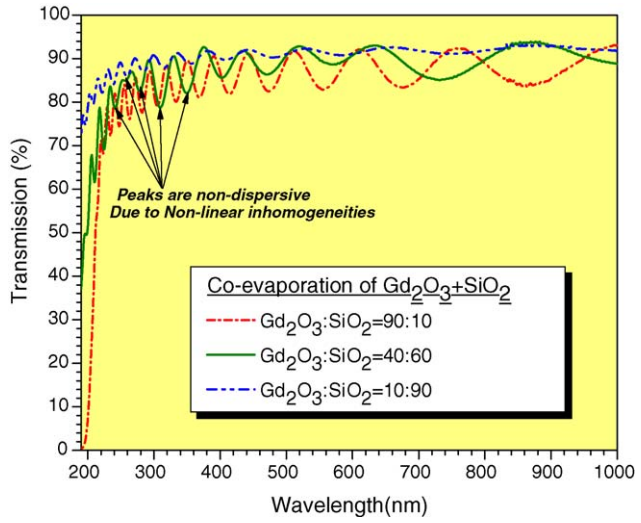

Fig. 4. Spectral transmittances of composite Gd_2O_3/SiO_2 thin films for the compositions of 90:10, 40:60 and 10:90. The transmittance curve for 40:60 (Gd_2O_3:SiO_2) composition displays interference peak modulation distinctly indicating inhomogeneity in the film growth properties.

mean spectral refractive index profile of the pure Gd_2O_3 film lies below that of the codeposited composite films with Gd_2O_3/SiO_2 mixing ratios of 90:10 and 80:20. This is a very interesting situation, which generates a possibility of attaining superior optical properties from a high index material by stabilizing it with silica components. Such a situation is only possible where microstructural and morphological densifications override the chemical compositions or the stoichiometry. The mean refractive spectral indices of all these films computed using Tauc–Lorentz (TL) formulations, effective medium approximations (EMA) and multilayer modeling approach. The results of all the codeposited composite films have been presented in Fig. 3. It is to be emphasized that in spite of microstructural inhomogeneities developed in thicker films, the mean refractive index profiles follow a very systematic trend as per the compositional mixings. Fig. 4 presents spectral transmission of three different codeposited films in which the respective transmittance amplitudes and band edge positions can be distinctly noticed. The spectral transmission for a Gd_2O_3/SiO_2 composition of 40:60 depicted non-dispersive peak amplitudes highlighting the growth dependent non-linear refractive index characteristics. These aspects are also highlighted from the ellipsometric measurements. The band gap analysis results of all these composite sample films using TL parameterizations have been presented in Fig. 5. It can be noticed from the plots that as expected, the higher the SiO_2 composition, the higher is the band gap. The highest band gap value of 7.7 eV has been obtained for the codeposited film that carries Gd_2O_3/SiO_2 compositions of 10:90. The band gap evolutions with respect to the mixing compositions have distinctly depicted a multi-slope behaviour. As pointed out earlier, it can be noticed from the spectrophotometric measurements that most of the films demonstrated some sort of microstructural inhomogeneities reflected in the spectral transmittance profiles. Such aspects

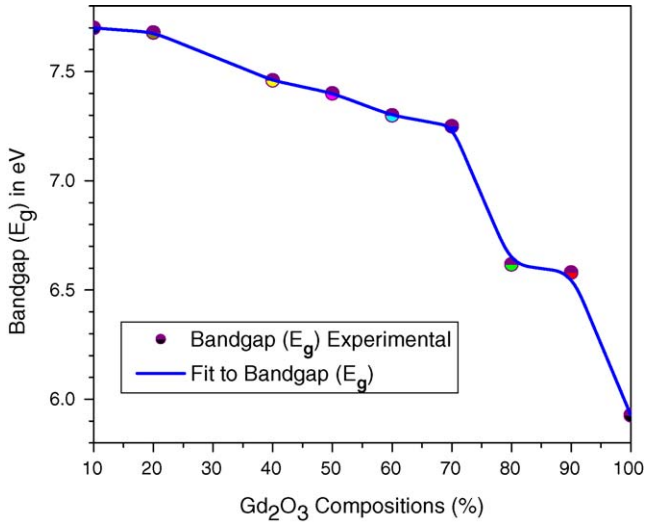

Fig. 5. Band gap values of the composite films with respect to various mixing ratios of Gd_2O_3 and SiO_2. As expected all the codeposited composite films depicted superior band gaps.

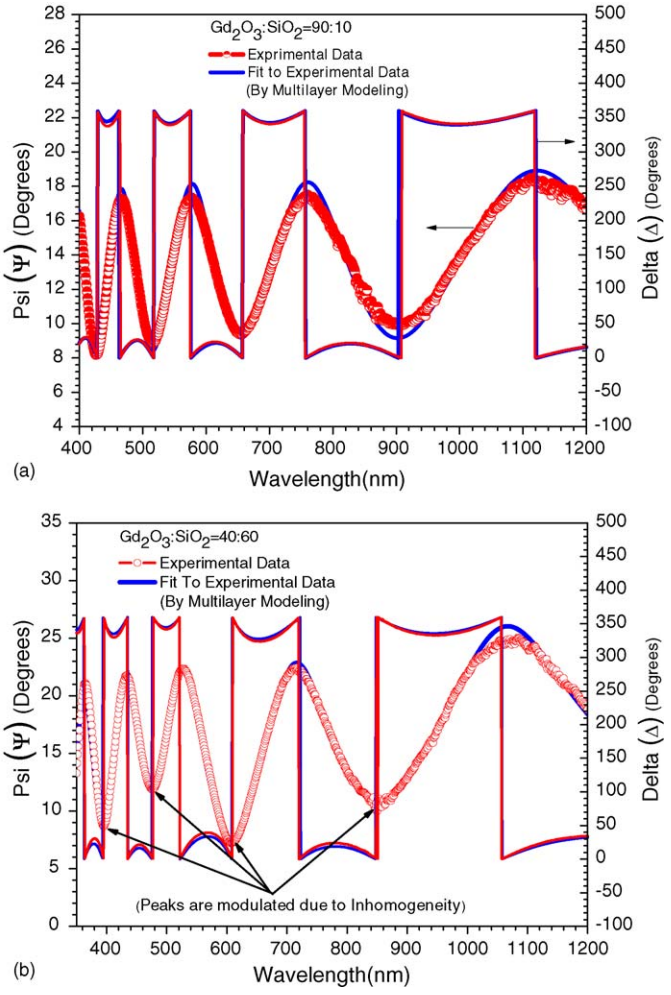

Fig. 6. Experimental and fitted ellipsometric data of the composite films with: (a) mixing ratio of 90:10 and (b) 40:60 of Gd_2O_3:SiO_2. In the mixing ratio of 40:60, the growth dependent non-linear properties are highlighted as spectral peak modulations of the Ψ parameter.

Table 1
Tauc–Lorentz (TL) model

Sample no.	Compositions Gd_2O_3:SiO_2	A (eV)	E_0 (eV)	E_g (eV)	C (eV)	ε_1
S30	10:90	200.00	12.30	7.7	0.000001	0.410
S29	20:80	171.21	12.49	7.68	0.013726	0.672
S28	40:60	192.75	11.80	7.46	0.000001	0.825
S27	50:50	202.00	11.80	7.40	0.00000001	0.564
S25	60:40	213.00	11.85	7.30	0.000001	0.711
S24	70:30	192.97	12.04	7.25	0.091331	0.795
S23	80:20	200.00	11.21	6.62	0.000001	0.342
S22	90:10	195.01	11.80	6.58	0.028252	0.300
Gd_2O_3	100:0	145.99	11.90	6.07	1.10	0.320

Tauc–Lorentz fitting parameters for the various codeposited composite Gd_2O_3/SiO_2 films as well as pure Gd_2O_3 film derived through ellipsometric analysis and modeling. The most important parameters A, E_g and C are related to the film density, band gap and the film disorder, respectively.

were highlighted in the ellipsometric measurements as well. The origin of these inhomogeneities can be ascribed to the process dependent microstructural growth as well as due to process instabilities. It is well known that such optical inhomogeneities are best tackled by appropriate discrete multilayer models [41–44]. In view of this, the analyses of the spectral ellipsometric parameters were carried out using a multilayer approach that suits best to the present sample films characteristics. The results of modeling using TL formulations are presented in Table 1. It can be seen from this table that the composite films have superior parameters representing film density and ordered structure in comparison to pure Gd_2O_3 films. It was noticed that most of the composite films could be modeled with five to eight sub-layers in the systems. The goodness of fit to the parameter Ψ and Δ justifies such a multilayer modeling approach. The results of two different composite films have been presented in Fig. 6(a and b). It can be

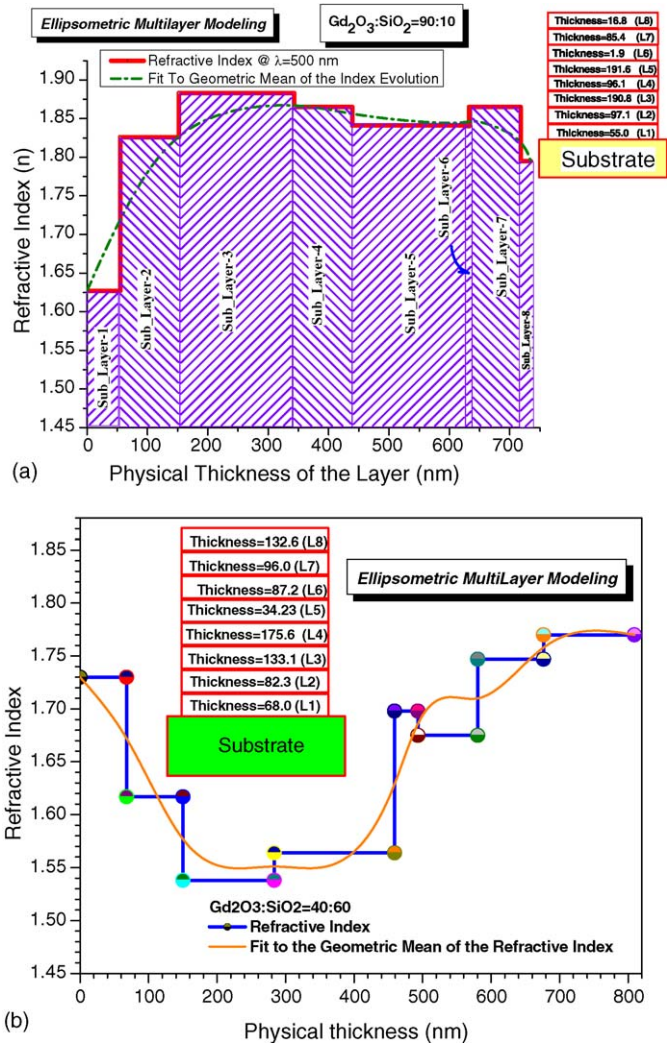

Fig. 7. Multilayer ellipsometric modeling of the composite films with: (a) mixing ratio of 90:10 and (b) 40:60 of Gd_2O_3:SiO_2. As expected the composite film with a mixing ratio of 40:60 depicted distinct non-linearity in the growth dependent non-linear refractive index profile.

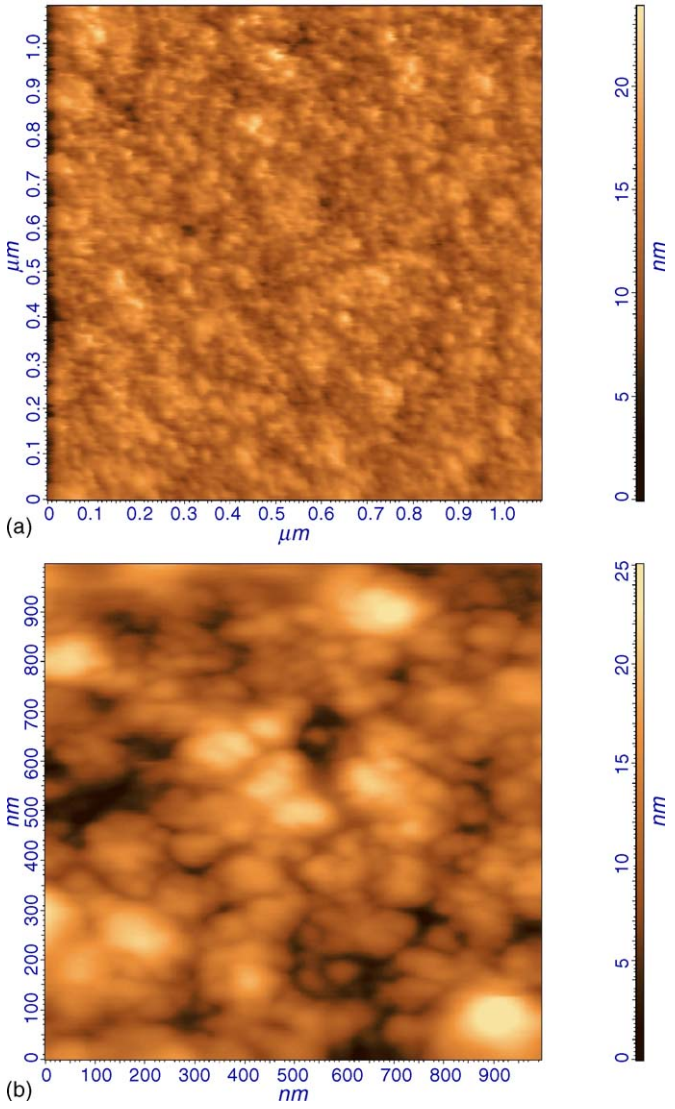

Fig. 8. Topographic properties of the composite film with: (a) mixing ratio of 90:10 and (b) pure Gd_2O_3 film. The mixed composite film has depicted a superior morphology with dense microstructure as compared to the pure Gd_2O_3 film.

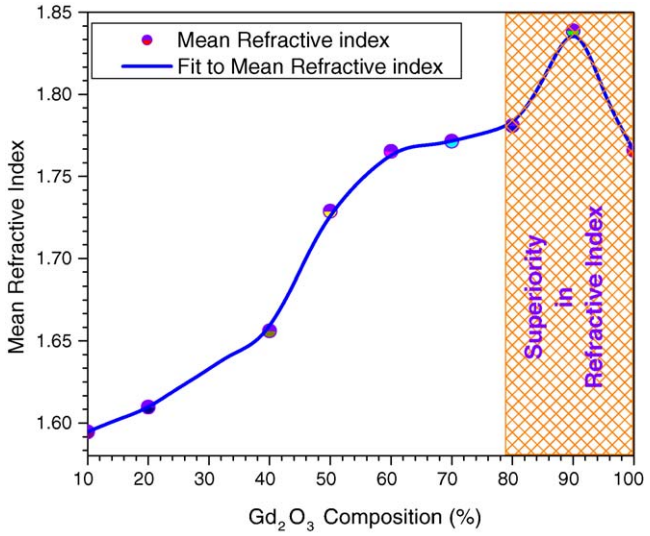

Fig. 9. Mean refractive index evolution of the composite films at a wavelength of 500 nm with respect to the various compositional mixing ratios. It can be noticed that the presence of certain amount of SiO_2 (10–20%) in the composite film has increased the effective refractive index values.

noticed from Fig. 6(b) that the plot of Ψ has demonstrated a non-dispersive spectral behaviour, which is dominantly due to the non-linear inhomogeneities appeared during the growth of this film. Fig. 7(a and b) depict the results of the multilayer models adopted for the above two composite films. Both the films have been modeled using eight (8) sub-layers in the system. Fig. 7(b) depicted a more prominent non-linearity in the growth of the refractive index profile. It is worth mentioning that such ellipsometric spectral characteristics cannot be fit using a single layer model. The topography results for pure Gd_2O_3 and codeposited films with Gd_2O_3:SiO_2 as 90:10 are presented in Fig. 8(a and b). It can be noticed that composite film at this composition of 90:10 has demonstrated superior morphology with a rms value of 3.53 nm in comparison to the pure thin films of Gd_2O_3, which has rms value 4.2 nm. The grains are much smaller and well packed compared to the pure Gd_2O_3 film. The interesting microstructural developments round about this composition need further investigations and task of our future plans. At present, however, it can be inferred that such a condition in superior film properties might be due to stabilization of thin film phase to a different one compared to the pure film. The mean spectral refractive index profile with respect to different Gd_2O_3/SiO_2 compositions is depicted in Fig. 9. It distinctly indicates a rise in the refractive index for the composition 90:10 that supports the morphological as well as ellipsometric results. Besides, this plot indicated a non-linear growth in the refractive index profile with respect to various compositions in the codeposited films.

5. Conclusion

The codeposited composite films of Gd_2O_3/SiO_2 have been analysed for their optical properties primarily by phase-modulated ellipsometry. The spectral refractive index profiles and band gap values of the films were derived from the Tauc–Lorentz formulations. Morphological properties have been acquired using a multimode scanning probe microscope technique. It was noticed that almost all the composite films have superior band gap as well as morphologies. The best optical parameters were obtained for the composite film that carries a mixing ratio of 90:10 of Gd_2O_3:SiO_2. Under this composition both the refractive index as well as band gap demonstrated superior numerical values with respect to the pure gadolinia films. The presence of 10–20% SiO_2 in gadolinia matrix has resulted into microstructural densifications as observed in some composite thin film systems. Such a composition required more probing in order to understand the superior film properties of the composite system. The compositional band gap variations have distinctly depicted different slopes in their evolutions with respect to the compositions. Such a result clearly indicates that microstructural properties do not follow a linear trend with respect to the mixing compositions. This behavior is due to the fact that the microstructure, which strongly affects opto-mechanical properties, does not vary linearly with composition. As pointed out earlier, factors such as bond strengths, chemical environment of the atoms and grains, surface mobility of the species during deposition and both short- and long-range order can induce a microstructure that is unique to the mixed composition film.

Acknowledgements

The authors wish to acknowledge the contribution of Mr. A. Biswas of Spectroscopy Division in carrying out ellipsometric measurements of all these samples and Mr. M. Senthilkumar for the AFM measurements. The authors also wish to acknowledge the support and encouragement of Dr. R.P. Shukla, former Head, Spectroscopy Division, Bhabha Atomic Research Centre, Mumbai during the course of this work.

References

[1] J.G. Yoon, H.K. Oh, Y.J. Kwag, J. Kor. Phys. Soc. 33 (1998) 699.
[2] W.H. Southwell, Appl. Opt. 24 (1985) 457.
[3] P.G. Verly, Appl. Opt. 37 (1998) 7327.
[4] J.M. Yang, C.Y. Kao, Appl. Opt. 40 (2001) 3256.
[5] R. Bertram, M.F. Ouellette, P.Y. Tse, Appl. Opt. 28 (1989) 2935.
[6] N.S. Gluck, H. Sankur, J. Heuer, J. DeNatale, W.J. Gunning, J. Appl. Phys. 69 (1991) 3037.
[7] R. Jacobson, J.O. Martensson, Appl. Opt. 5 (1966) 29.
[8] P. Camagni, P. Galinetto, G. Samoggia, Solid State Commun. 83 (1992) 943.
[9] M.A. Taylor, M. Kilo, G. Borchardt, S. Weber, H. Scherrer, J. Eur. Ceram. Soc. 25 (2005) 1591.
[10] G.A. Niklasson, C.G. Granqvist, O. Hunderi, Appl. Opt. 20 (1981) 26.
[11] H. Sankur, W. Gunning, J. DeNatale, Appl. Opt. 27 (1988) 1564.
[12] A. Alvarez-Herrero, G. Ramos, F. del Monte, E. Bernabeu, D. Levy, Thin Solid Films 455–456 (2004) 356.
[13] V.V. Kriventsova, D.I. Kochubeya, M.V. Tsodikovb, J.A. Navioc, G.M. Restrepod, M. Maciasc, Nucl. Instrum. Meth. Phys. Res. A 470 (2001) 347.
[14] H. Sankur, W. Gunning, J. Appl. Phys. 66 (1989) 807.
[15] E.N. Farabaugh, E.M. Sanders, J. Vac. Sci. Technol. A 1 (1983) 356.
[16] E.N. Farabaugh, A. Feldman, J. Sun, Y.N. Sun, J. Vac. Sci. Technol. A 5 (1987) 1671.
[17] H. Sankur, W. Gunning, J. Appl. Phys. 66 (1989) 4747.

[18] D.G. Howitt, A.B. Harker, J. Mater. Sci. 2 (1987) 201.
[19] N.K. Sahoo, M. Senthilkumar, S. Thakur, D. Bhattacharyya, Appl. Surf. Sci. 200 (2002) 219.
[20] N.K. Sahoo, S. Thakur, M. Senthilkumar, D. Bhattacharyya, N.C. Das, Thin Solid Films 440 (2003) 155.
[21] A.A. Dakhel, J. Opt. A, Pure Appl. Opt. 3 (2001) 452.
[22] B. Bates, D.J. Bradley, Appl. Opt. 5 (1966) 971.
[23] A.P. Bradford, G. Hass, J.F. Osantowski, A.R. Tort, Appl. Opt. 8 (1969) 1183.
[24] F. Rainer, W.H. Lowdermilk, D. Milam, C.K. Carniglia, T.T. Hart, T.L. Lichtenstein, Appl. Opt. 24 (1985) 496.
[25] E. Quesnel, L. Dumas, D. Jacob, F. Peiró, J. Vac. Sci. Technol. A 18 (2000) 2869.
[26] E. Eva, K. Mann, N. Kaiser, B. Anton, R. Henking, D. Ristau, P. Weissbrodt, D. Mademann, L. Raupach, E. Hacker, Appl. Opt. 35 (1996) 5613.
[27] A. Portinha, V. Teixeira, J. Carneiroa, M.F. Costa, N.P. Barradas, A.D. Sequeira, Surf. Coat. Technol. 188–189 (2004) 107.
[28] H. Lee, I.Y. Kim, S.S. Han, B.S. Bae, M.K. Choi, I.S. Yang, J. Appl. Phys. 90 (2001) 813.
[29] A.V. Osipov, F. Schmitt, P. Hess, Thin Solid Films 472 (2005) 31.
[30] Y.J. Cho, N.V. Nguyen, C.A. Richter, J.R. Ehrstein, B.H. Lee, J.C. Lee, Appl. Phys. Lett. 80 (2002) 1249.
[31] B. von Blanckenhagen, D. Tonova, J. Ullmann, Appl. Opt. 41 (2002) 3137.
[32] H. Chen, W.Z. Shena, Eur. Phys. J. B 43 (2005) 503.
[33] A.C. Diebold, J. Canterbury, W. Chism, C. Richter, N. Nguyen, J. Ehrstein, C. Weintraub, Mater. Sci. Semicond. Process. 4 (2001) 3.
[34] G.E. Jellison Jr., V.I. Merkulov, A.A. Puretzky, D.B. Geohegan, G. Eres, D.H. Lowndes, J.B. Caughman, Thin Solid Films 377–378 (2000) 68.
[35] G.E. Jellison Jr., F.A. Modine, Appl. Phys. Lett. 69 (1996) 371.
[36] R. Jacobson, Inhomogeneous and coevaporated homogeneous films for optical applications, in: G. Hass, M.H. Francombe, R.W. Hoffman (Eds.), Physics of Thin Films, vol. 8, Academic Press, New York, 1975, pp. 51–98.
[37] N. Jun, G. Binglin, Comp. Phys. Commun. 147 (2002) 234.
[38] A. Feldman, E.N. Farabaugh, W.K. Haller, D.M. Sanders, R.A. Stempniak, J. Vac. Sci. Technol. A 4 (1986) 2969.
[39] F. Tcheliebou, A. Boyer, L. Martin, Thin Solid Films 249 (1994) 86.
[40] W.H. Koo, S.M. Jeong, S.H. Choi, H.K. Baik, S.J. Lee, S.M. Lee, J. Vac. Sci. Technol. A 22 (2004) 2048.
[41] A.V. Tikhonravov, M.K. Trubetskov, A.V. Krasilnikova, Appl. Opt. 37 (1998) 5902.
[42] P. Chindaudom, K. Vedam, Appl. Opt. 33 (1994) 2664.
[43] G.P. de Lariviere, J.M. Frigerio, J. Rivory, F. Abeles, Appl. Opt. 31 (1992) 6056.
[44] A.V. Tikhonravov, M.K. Trubetskov, B.T. Sullivan, J.A. Dobrowolski, Appl. Opt. 36 (1997) 7188.